

## CHEMISTRY

# Miniature high-throughput chemosensing of yield, ee, and absolute configuration from crude reaction mixtures

Keith W. Bentley, Peng Zhang, Christian Wolf\*

2016 © The Authors, some rights reserved; exclusive licensee American Association for the Advancement of Science. Distributed under a Creative Commons Attribution NonCommercial License 4.0 (CC BY-NC). 10.1126/sciadv.1501162

High-throughput experimentation (HTE) has emerged as a widely used technology that accelerates discovery and optimization processes with parallel small-scale reaction setups. A high-throughput screening (HTS) method capable of comprehensive analysis of crude asymmetric reaction mixtures (eliminating product derivatization or isolation) would provide transformative impact by matching the pace of HTE. We report how spontaneous in situ construction of stereodynamic metal probes from readily available, inexpensive starting materials can be applied to chiroptical chemosensing of the total amount, enantiomeric excess (ee), and absolute configuration of a wide variety of amines, diamines, amino alcohols, amino acids, carboxylic acids,  $\alpha$ -hydroxy acids, and diols. This advance and HTS potential are highlighted with the analysis of 1 mg of crude reaction mixtures of a catalytic asymmetric reaction. This operationally simple assay uses a robust mix-and-measure protocol, is amenable to microscale platforms and automation, and provides critical time efficiency and sustainability advantages over traditional serial methods.

## INTRODUCTION

It has become routine in academic and industrial laboratories to conduct hundreds of reactions in parallel using modern high-throughput experimentation (HTE) technology (1, 2). However, the analysis of hundreds of asymmetric reactions remains challenging because costs, time pressure, minute sample amounts, and waste management issues need to be considered. The constant quest for new chiral pharmaceuticals, agrochemicals, and other biologically active compounds continues to increase the universal demand for analytical means that effectively support asymmetric synthesis development and optimization efforts (3). However, the determination of the reaction yield and enantiomeric excess (ee) by traditional methods has remained time-consuming and costly, and the mismatch in the throughput of generally available synthetic and analytical tools has led to a growing interest in conceptually new screening approaches (4). To fully exploit the impact of HTE and to streamline serendipitous asymmetric reaction development, screening methods that are compatible with modern workflow platforms and time constraints, minimize waste production and operational (consumables and labor) costs, and are applicable to automated parallel analysis of hundreds of small-scale reactions are required. Groundbreaking steps toward this goal have been made with the introduction of one pot–multisubstrate–one catalyst experiments that are typically combined with traditional serial analysis such as gas chromatography–mass spectrometry (GC-MS) or high-performance liquid chromatography–ultraviolet detection (HPLC-UV) (5–7), infrared radiation (IR) (8), nuclear magnetic resonance (NMR) (9, 10), and MS methods (11–13) or biochemical assays (14–16). In addition, the potential of chiroptical methods has attracted increasing attention (17, 18).

Kurtán *et al.* (19), Nieto *et al.* (20), You *et al.* (21), Anyika *et al.* (22), Joyce *et al.* (23), our group (24, 25), and others (26, 27) have developed stereodynamic sensors that generate strong circular dichroism (CD) signals upon recognition of a chiral substrate. The utility of optical

chemosensors is generally tested with chemically pure, nonracemic samples to avoid interference from other compounds. This provides important information about the accuracy, sensitivity, and substrate scope of a sensing assay. However, it excludes possible interference from other compounds and therefore does not reveal the real potential for analysis of asymmetric reactions, which typically contain starting materials, by-products, catalysts, additives, etc., in addition to the sensing target. Few cases of specialized sensing applications have been reported. Li *et al.*, Matsumoto *et al.*, and our group used fluorosensors to determine the enantioselectivity of the asymmetric titanium tartrate-catalyzed addition of trimethylsilyl cyanide to an immobilized aldehyde (28), the kinetic resolution of a nitroaldol product tagged with a fluorescence probe (29), and the enzymatic kinetic resolution of *trans*-1,2-diaminocyclohexane, respectively (30). Leung *et al.* applied a UV indicator displacement assay to the stereochemical analysis of a diastereoselective Strecker reaction (31) and demonstrated that the ee and concentration of reductive amination products or of hydrobenzoin generated by asymmetric dihydroxylation (AD) can be determined after derivatization or isolation followed by artificial neural network data analysis (32, 33). Joyce *et al.* (34) recently reported the use of 3-hydroxypyridine-2-carboxaldehyde as CD sensor for ee determination of an enzymatic transamination. These pioneering steps toward high-throughput screening (HTS) of asymmetric reactions were, in some cases, limited to immobilized or tagged substrates, which increases the overall workload and can interfere with the reaction outcome; product derivatization or isolation steps were generally necessary before the analysis.

We believe that quantitative chemosensing of chiral compounds with stereodynamic metal complexes is particularly practical and bears unprecedented promise for HTS applications (35, 36). We now introduce bis(2-hydroxy-1-naphthyl)ketone, **1**, and show that it forms stereodynamic Al, Zn, and Ti complexes that can be used for the determination of absolute configuration, ee, and concentration, which we refer to as comprehensive chirality sensing (CCS). The concept of CCS with metal complexes of **1** is applicable to a large variety of chiral substrates and allows accurate reaction analysis without laborious product isolation

Chemistry Department, Georgetown University, Washington, DC 20057, USA.

\*Corresponding author. E-mail: cw27@georgetown.edu

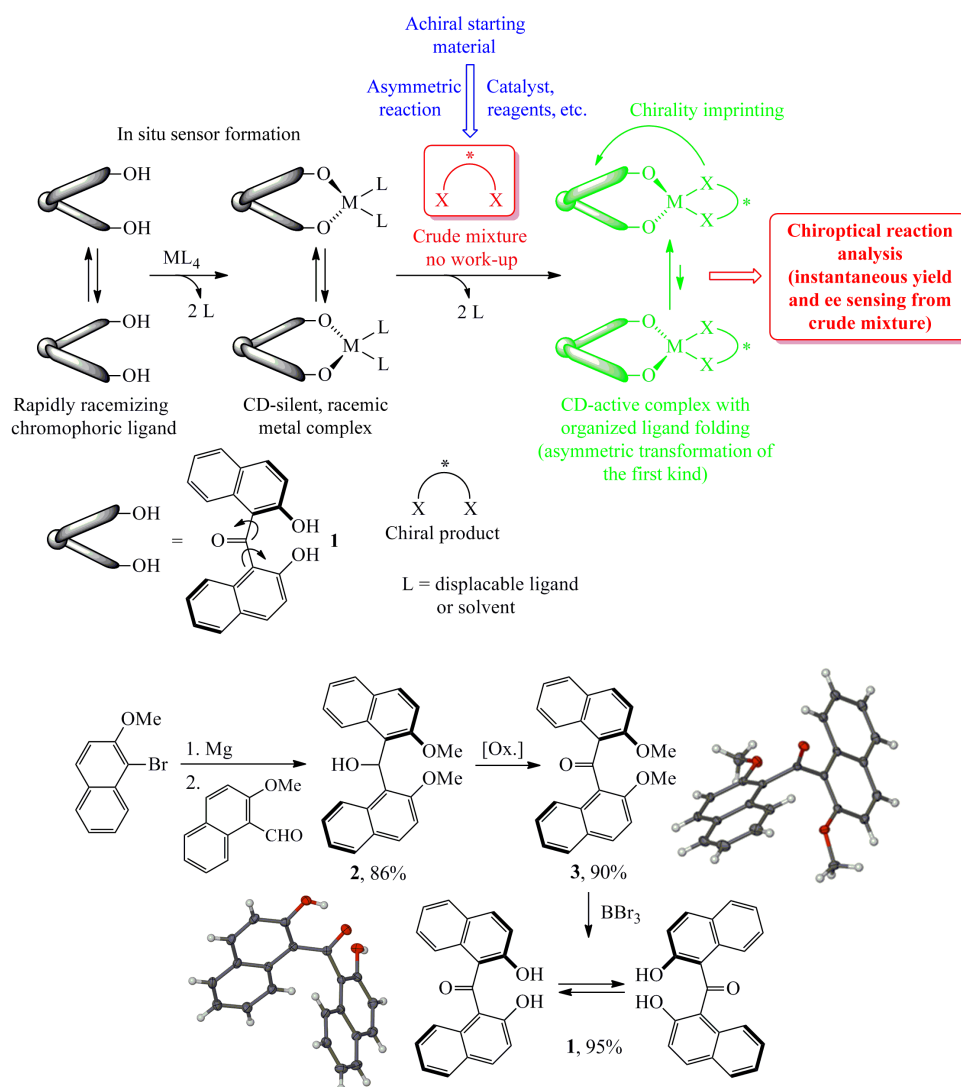
or derivatization. Chiral amines, diamines, amino acids, carboxylic acids, hydroxy acids, and diols can be quantitatively analyzed with a simple mix-and-measure protocol. We highlight the potential of this approach by applying the titanium complex of **1** in direct ee and yield analyses using crude reaction mixtures of the Sharpless AD of *trans*-stilbene, and demonstrate significant time and sustainability advantages over conventional reaction analysis.

## RESULTS AND DISCUSSION

### Probe design and CCS with a stereodynamic zinc complex

We show the underlying principles of our CCS method in Scheme 1. We envisioned that **1** would instantly form stable metal complexes that exist as a racemic and therefore CD silent mixture of rapidly interconverting enantiomers. Coordination of a chiral substrate disturbs this equilibrium and favors formation of one diastereomer through asym-

metric transformation of the first kind. The binding event and the instantaneous chiral induction result in a fluorescence change and an induced CD (ICD) signal, which are quantitatively correlated to the substrate amount and ee, respectively. We prepared **1** in three high-yielding steps (Scheme 1 and Supplementary Materials). We then tested the potential of stereodynamic chirality sensing with ligand **1** using a stoichiometric amount of Et<sub>2</sub>Zn and enantiopure *trans*-1,2-diphenylethylenediamine, **4**. The complex formation between **1** and Et<sub>2</sub>Zn and the subsequent coordination of the diamine substrate occurred spontaneously and gave quantitative amounts of the dinuclear species (**1**-Zn-**4**)<sub>2</sub> according to MS analysis (see the Supplementary Materials). We observed a very strong CD signal of the in situ–formed complex at high wavelength at a concentration of 1 mM in diethyl ether, and similar CD responses to other aliphatic and aromatic amines **5** to **8** were obtained (Fig. 1). Additional CD sensing experiments revealed a remarkably broad substrate scope, including amino alcohols **9** to **14** and amino acids **15** to **18**. All sensing experiments were conducted



**Scheme 1.** Concept of chirality sensing and asymmetric reaction analysis with a stereodynamic CD/fluorescence chemosensor and synthesis of bis(2-hydroxy-1-naphthyl)ketone, **1**.

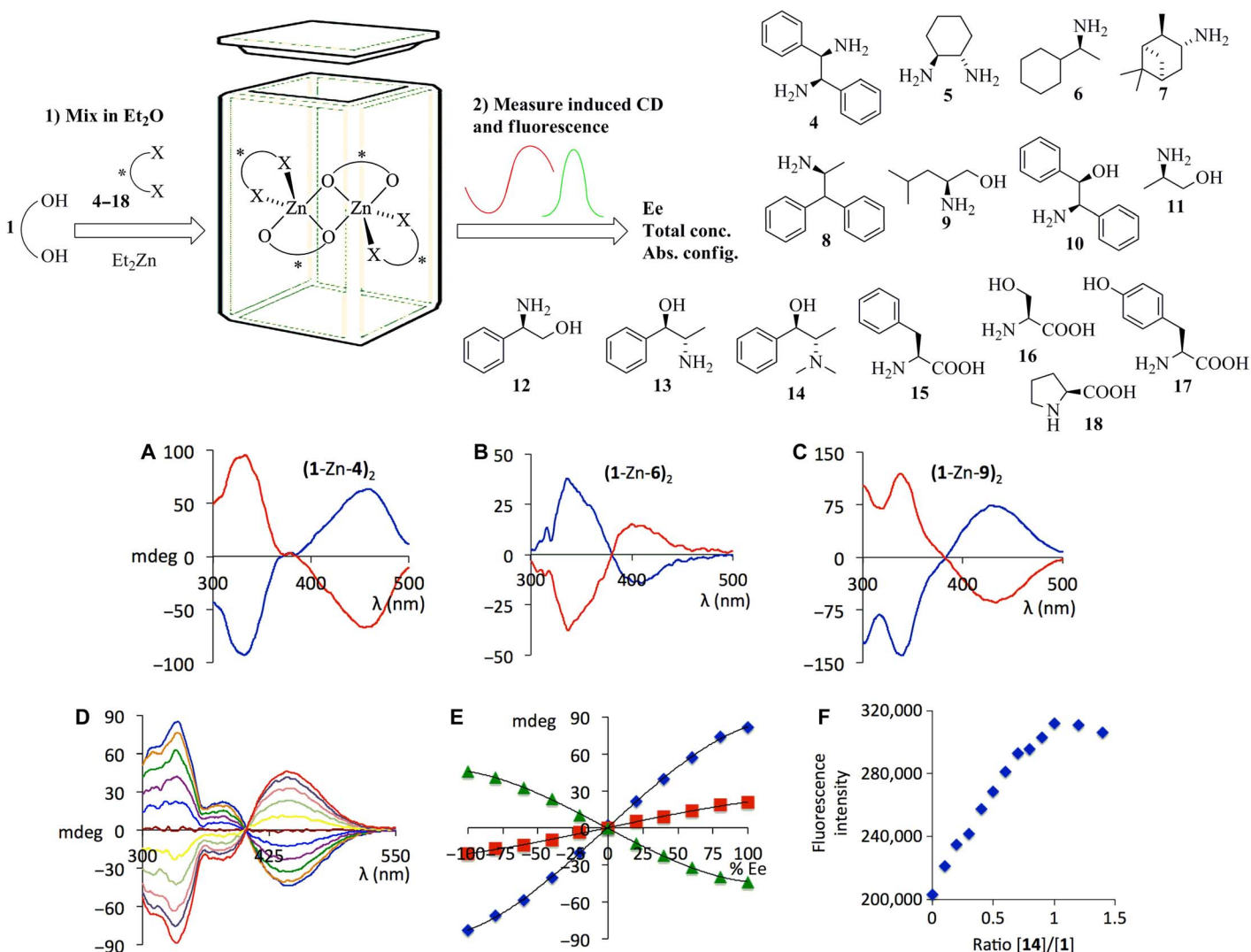


**Fig. 1. Chiroptical sensing of amines, amino alcohols, and amino acids.** Top: General CD sensing scheme and substrate scope (only one enantiomer of each substrate is shown) of the zinc complex of **1**. Middle: (A) CD spectra of the Zn complex derived from **1** and (1*R*,2*R*)-**4** (blue) and (1*S*,2*S*)-**4** (red). (B) CD response to (*R*)-**6** (blue) and (*S*)-**6** (red). (C) CD response to (*R*)-**9** (blue) and (*S*)-**9** (red). Bottom: (D) CD spectra of the Zn complex derived from **1** and non-racemic samples of **14**. (E) Plots of the CD amplitudes at 338 nm (blue), 385 nm (red), and 445 nm (green) versus ee. (F) Plot of the fluorescence intensity of the Zn complex derived from **1** and varying equivalents of **14**. All CD spectra were collected at 1 mM in diethyl ether.

using a simple mix-and-measure protocol, pipetting tetrahydrofuran (THF) solutions of **1**, **4**, or another substrate, and finally, Et<sub>2</sub>Zn (in hexanes) in air into small vials as indicated in Fig. 1. Solutions were further diluted with THF and subjected to CD analysis within a few minutes. Careful inspection of the spectra shows that the absolute configuration of each substrate can be determined from the sign of the ICD maximum at 425 nm. The *R* enantiomers of amines and amino acids afford a negative CD amplitude, whereas a positive CD effect is induced upon addition of the *S* enantiomers. Amino alcohols and diamines exhibit the opposite relationship between the chiroptical sensor readout and the absolute configuration of the substrate (see the Supplementary Materials).

To evaluate the possibility of fast ee sensing, we collected CD spectra of the Zn complex of **1** and varying enantiomeric composition of *N*-methyl ephedrine **14** (Fig. 1, D and E). Plots of the sensor ICD re-

sponses versus substrate ee at three different wavelengths consistently showed a sigmoidal relationship, which can be attributed to coexisting  $\mu$ -oxo-bridged homo- and heterochiral (1-Zn-**14**)<sub>2</sub> species in solution (36). Indeed, electrospray ionization (ESI)-MS analysis confirmed the formation of a dinuclear complex of **1**, Zn, and amino alcohols including **14** with a [2:2:2] stoichiometry (see the Supplementary Materials). This explains the observed nonlinear CD responses of our sensor, and it compares well with nonlinear effects (NLEs) commonly encountered in asymmetric reactions with chiral catalysts prepared from diethylzinc and amino alcohols or other ligands (37, 38). We then tested the suitability of the stereodynamic Zn complex for quantitative chirality sensing. We were pleased to find that a simple mix-and-measure protocol with several nonracemic samples of **14** gave accurate results (Table 1). The averaged ee values calculated from the responses at three different wavelengths were within 2.2% of the actual value.

**Table 1.** CCS of *N*-methyl ephedrine **14**.

Sample composition				Chemosensing results					
Entry	Ee (%)	Conc. (mM)	Abs. config.	Ee (%), 338 nm	Ee (%), 385 nm	Ee (%), 445 nm	Ee (%), avg.	Conc. (mM)	Abs. config.
1	87.0	0.56	<i>R</i>	85.4	89.5	82.6	85.8	0.60	<i>R</i>
2	76.0	1.01	<i>R</i>	78.5	79.3	76.7	78.2	1.09	<i>R</i>
3	26.0	2.36	<i>S</i>	27.2	22.5	24.3	24.7	2.29	<i>S</i>
4	68.0	2.93	<i>S</i>	70.2	65.3	64.8	66.8	2.96	<i>S</i>
5	89.0	3.34	<i>S</i>	90.6	86.9	84.2	87.2	3.38	<i>S</i>

Moreover, the binding of **14** to the Zn complex of **1** results in fluorescence enhancement in addition to the ICD effect. Unlike the enantioselective CD response of our sensor to the ee of **14** or other chiral substrates, the change in the fluorescence readout is not enantioselective and therefore independent of the substrate ee. The strongest fluorescence intensity was measured when an equimolar amount of **14** was present, and substrate excess did not further alter the fluorescence output of the sensor (Fig. 1F and Supplementary Materials). This nonenantioselective fluorescence sensor output can be used for accurate determination of the total substrate concentration of **14** (Table 1).

#### CCS with aluminum and titanium complexes of **1**

The use of ligand **1** for chirality sensing is not limited to zinc complexes. The formation of an aluminum complex with Me<sub>3</sub>Al and **1** provides an entry to chemosensing of chiral  $\alpha$ -hydroxy acids and carboxylic acids (Fig. 2 and Supplementary Materials). Again, the CD response of the stereodynamic metal complex can be systematically correlated to the absolute configuration of the substrates. The *R* enantiomers of  $\alpha$ -hydroxy acids yield a positive CD sensor response at 450 nm, whereas *S* enantiomers give a negative signal. We observed the opposite trend with carboxylic acids (see the Supplementary Materials). In analogy to the zinc complex discussed above, **1** appears to form dinuclear aluminum complexes according to ESI-MS analysis (see the Supplementary Materials).

The general utility of the zinc and aluminum complexes of ligand **1** for chirality chemosensing of amines, amino alcohols, amino acids,  $\alpha$ -hydroxy acids, and carboxylic acids encouraged us to further evaluate this tropos ligand. We were pleased to find that chiral 1,2-, 1,3-, and even 1,4-diols generate a distinctive ICD response to the Ti complex of **1** (Fig. 2C and Supplementary Materials). Again, nonenantioselective fluorescence enhancement was observed as the substrate amount was steadily increased to an equimolar amount, and no further change was observed in the presence of excess of **25**. We conducted ee and concentration analyses as described above with hydrobenzoin **25** as substrate (Fig. 2, D to G). In analogy to the quantitative chirality chemosensing of amino alcohol **14** with the stereodynamic zinc binaphtholate complex, we observed that the CD and fluorescence responses of the titanium complex formed in situ from **1** can be used for fast determination of the enantiomeric purity and the amount of nonracemic samples of **25** covering a wide ee and concentration range (Table 2).

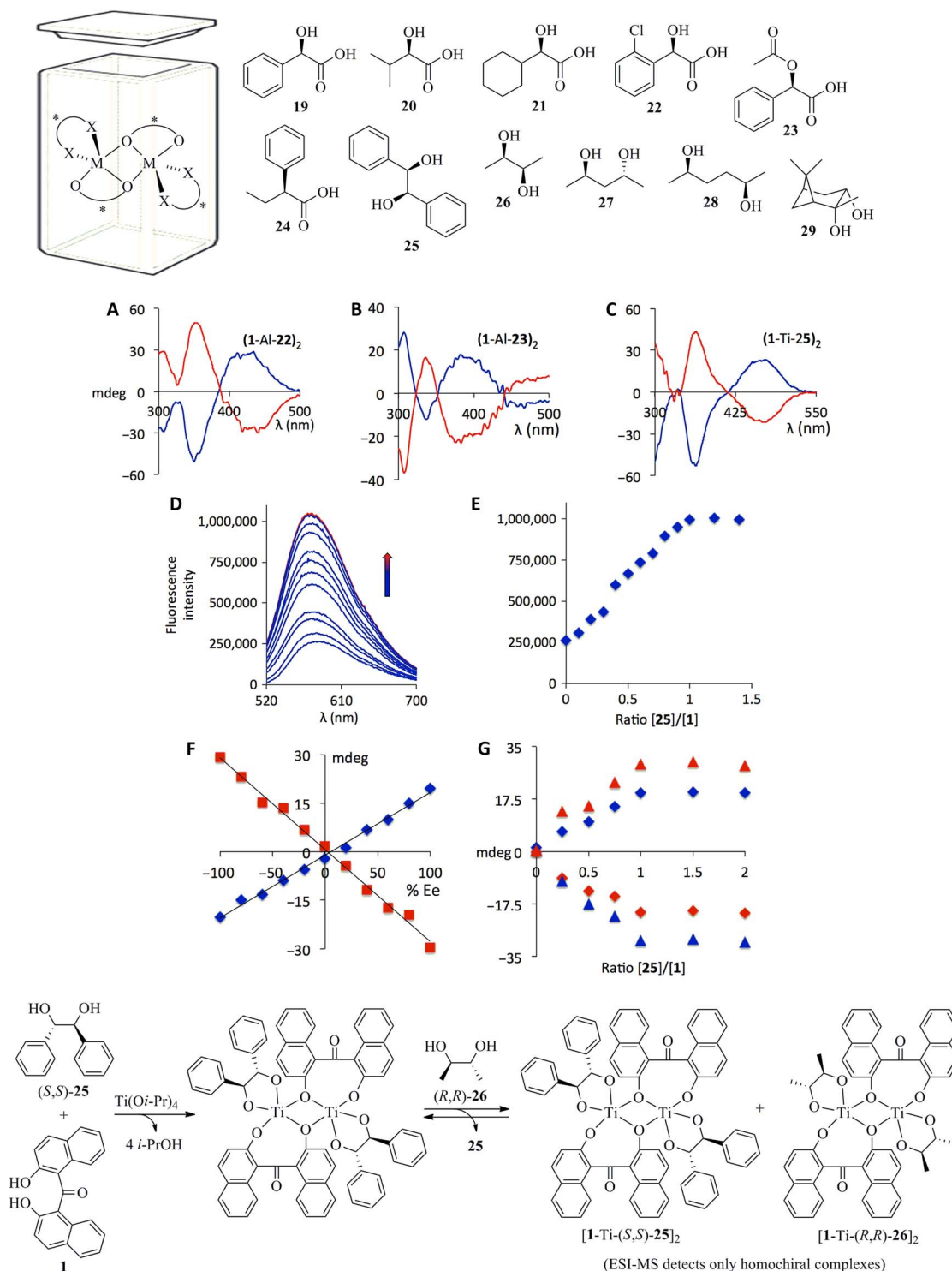
As shown in Fig. 2F, we obtained a linear CD response to the substrate ee at two distinct wavelengths, which is in contrast to the chiroptical NLE of the zinc complex described above. Although the linear

CD effect could be attributed to a monomeric metal complex (39), it is known that diphenolate- and binaphtholate-derived titanium complexes typically form  $\mu$ -oxo-bridged dinuclear structures and often exhibit dynamic equilibria of higher aggregates (40). We observed only a signal of ternary (1-Ti-25)<sub>2</sub> by ESI-MS and detected no sign of the mononuclear analog, higher aggregates, and binary Ti complexes carrying either only **1** or **25** (see the Supplementary Materials). NMR analysis at 25°C and low temperatures showed broad resonances in the aromatic region indicating a mixture of interconverting species, and titration analysis with Ti(O*i*-Pr)<sub>4</sub> proved consecutive substitution of all four isopropoxides upon coordination of **1** and **25** (see the Supplementary Materials). The fluorescence signal and the CD intensities of (1-Ti-25)<sub>2</sub> did not change in the presence of excess of **25** (Fig. 2, D, E, and G, and Supplementary Materials), which is in excellent agreement with the ESI-MS results. Together, these observations support predominant formation of (1-Ti-25)<sub>2</sub> under thermodynamic control; that is, the observed chiral amplification and ICD signal are a result of asymmetric transformation of the first kind. As discussed above, the appearance of dinuclear complexes such as (1-Zn-14)<sub>2</sub> typically results in nonlinear chiroptical effects (Fig. 1E). With regard to the dinuclear Ti complexes, we found evidence that the perfectly linear correlation between the ICD effect and the ee of the diol substrate shown in Fig. 2F originates from a thermodynamic preference for the homochiral versus the heterochiral (1-Ti-25)<sub>2</sub> species. To differentiate between homo- and heterochiral complexes, we designed ESI-MS exchange experiments using (*S,S*)-**25**, Ti(O*i*-Pr)<sub>4</sub>, and either enantiomer of the diol **26**. In agreement with the NMR, CD, and fluorescence data described above, the ESI-MS results suggest that the diol ligands can be exchanged from the Ti center, whereas the ICD reporter ligand **1** is not replaced. The addition of (*R,R*)-**26** to [1-Ti-(*S,S*)-**25**]<sub>2</sub> indeed gave a mixture of the two homochiral complexes [1-Ti-(*S,S*)-**25**]<sub>2</sub> and [1-Ti-(*R,R*)-**26**]<sub>2</sub>, which appeared with similar intensities, whereas the intermediate heterochiral Ti complex containing both (*S,S*)-**25** and (*R,R*)-**26** was not detected (Fig. 2 and Supplementary Materials). In contrast, the homochiral dinuclear Ti complex containing one molecule of each diol was observed by MS when (*S,S*)-**25** and (*S,S*)-**26** were used. The results of our ESI-MS ligand exchange experiments thus suggest that the homochiral Ti complex is more stable than the heterochiral analog, which explains the linear ICD effect observed for the diol ee sensing.

#### CCS of crude materials from an asymmetric reaction

The general practicality and time efficiency of chirality sensing with stereodynamic metal complexes of ligand **1** led us to use the titanium

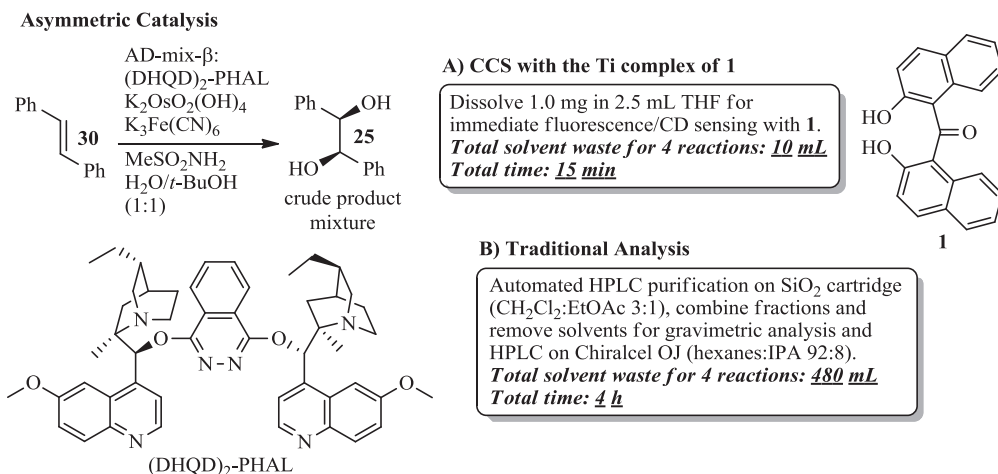




**Fig. 2. Chiroptical sensing of carboxylic acids, hydroxy acids, and diols.** Top: Substrate scope using **1** with Me<sub>3</sub>Al (**19** to **24**) or Ti(Oi-Pr)<sub>4</sub> (**25** to **29**). Only one enantiomer is shown. Middle: **(A)** CD spectra of the Al complex derived from **1** and (*R*)-**22** (blue) and (*S*)-**22** (red). **(B)** Sensor response to the Ti complex derived from **1** and (*R,R*)-**25** (blue) and (*S,S*)-**25** (red). An equivalent of Et<sub>3</sub>N was added to  $\alpha$ -hydroxy acids before analysis. **(D)** Fluorescence intensity of the Ti complex derived from **1** and varying molar equivalents of **25**. **(E)** Plot of the fluorescence intensity at 600 nm of the Ti complex derived from **1** and varying amounts of **25**. **(F)** Plots of the ICD amplitudes at 375 nm (red) and 470 nm (blue) for the Ti complex derived from **1** and nonracemic samples of **25**. **(G)** ICD intensity at 375 nm (triangles) and 470 nm (diamonds) for the complex obtained from Ti(Oi-Pr)<sub>4</sub>, **1**, and various amounts of (*R,R*)-**25** (blue) and (*S,S*)-**25** (red). All spectra were collected at 1 mM in diethyl ether. Bottom: Thermodynamically controlled Ti complex formation and equilibrium between homochiral species observed by ESI-MS using (*S,S*)-**25** and (*R,R*)-**26**.

**Table 2.** CCS of hydrobenzoin **25**, using **1** and Ti(O*i*-Pr)<sub>4</sub>.

Sample composition				Chemosensing results				
Entry	Ee (%)	Conc. (mM)	Abs. config.	Ee (%), 375 nm	Ee (%), 470 nm	Ee (%), avg.	Conc. (mM)	Abs. config.
1	76.0	0.56	<i>R,R</i>	79.7	79.3	79.5	0.53	<i>R,R</i>
2	68.0	1.01	<i>R,R</i>	70.5	66.9	68.7	1.01	<i>R,R</i>
3	12.0	1.76	<i>R,R</i>	13.6	12.6	13.1	1.88	<i>R,R</i>
4	26.0	2.36	<i>S,S</i>	24.2	22.3	23.3	2.47	<i>S,S</i>
5	89.0	2.93	<i>S,S</i>	91.3	86.8	89.1	2.72	<i>S,S</i>

**Table 3.** Comparison of the yield, ee, and absolute configuration of hydrobenzoin obtained by AD of stilbene.

Sharpless AD			Traditional analysis		Chiroptical sensing	
Entry	Catalyst	T (°C)	Yield (%)	Ee (%) and abs. config.	Yield (%)	Ee (%) and abs. config.
1	AD-mix-β	0.0	99.1	99.1 ( <i>R,R</i> )	95.4	98.9 ( <i>R,R</i> )
2	AD-mix-β	25.0	71.0	86.3 ( <i>R,R</i> )	65.3	87.7 ( <i>R,R</i> )
3	AD-mix-β	50.0	17.7	75.4 ( <i>R,R</i> )	12.2	75.8 ( <i>R,R</i> )
4	Cinchonine	25.0	54.2	0.0 (n/a)	51.1	1.3 (n/a)

sensor in an important real-case application. We selected the Sharpless AD to test the usefulness of our sensing method for analysis of the yield and ee of an asymmetric reaction. We conducted four variations of the oxidation of *trans*-stilbene **30** to hydrobenzoin **25**, following a standard literature procedure (41). Upon completion, the titanium sensor complex was simply added to a THF solution containing 1 mg of the crude AD product and subjected to CD and fluorescence analyses (Table 3). Two fast measurements of the characteristic CD and fluorescence responses of the sensor using a single sample allowed accurate determination of the yield, ee, and absolute configuration of the major enantiomer formed. The sensing analysis proved straightforward and did not require recalibration of the previously determined probe readouts. Comparison with traditional analysis (gravimetry and chiral HPLC) of isolated **25** highlights that chiroptical sensing is a practical alternative with real HTS potential. The yields and, in particular,

the ee's vary only by a few percent, and the small deviation can probably be further reduced by using automated pipetting equipment, which is common in HTS settings. Nevertheless, the results are generally considered sufficiently accurate for HTS purposes. Errors up to 10% can be tolerated because the purpose of HTS is typically to uncover trends and to identify efficient reactions that afford >90% yield and >90% ee, for example, the Sharpless AD method shown in entry 1. The dual sensing approach (ee and fluorescence) with ligand **1** is fast, robust, and reproducible and allows analysis of minute amounts of a crude reaction mixture while laborious product derivatization or isolation procedures are avoided. The total time and solvent amount required for the analysis of the four AD reactions by chiroptical sensing were 15 min and 10 ml, respectively. This compares favorably with the 4 hours and 480 ml needed for the traditional analysis performed with an automated HPLC purification system. It is noteworthy that screening

of hundreds of samples would barely increase the total time required for CCS, which can be conducted in parallel and is adaptable to automation.

## CONCLUSION

In summary, we have discussed the concept of CCS with stereodynamic Zn, Al, and Ti complexes carrying a simple reporter ligand for fast analysis of minute sample amounts of a wide variety of chiral target compounds. The chiroptical probes are conveniently formed in situ, and the general application scope includes, but is not limited to, 26 chiral amines, diamines, amino alcohols, amino acids, carboxylic acids,  $\alpha$ -hydroxy acids, and diols. The substrate recognition and chiral amplification processes generate strong CD and fluorescence signals that were systematically correlated to the absolute configuration, ee, and concentration of the analytes tested. We demonstrated the general utility and accuracy of chiroptical chemosensing with the direct analysis (eliminating product derivatization and isolation) of 1 mg of crude reaction mixtures of the catalytic AD of *trans*-stilbene using a simple and robust mix-and-measure protocol that does not require recalibration of the chiroptical sensor readouts. This case study highlights how chiroptical chemosensing provides an effective means for fast screening of crude reaction mixtures together with a critical sustainability advantage over traditional chromatographic methods as a result of reduced solvent and energy consumption. The chiroptical sensing method holds considerable promise for HTE applications and other asymmetric reactions. For example, it could be applied to HTS of reactions yielding free amines or  $\alpha$ -hydroxy carboxylic acids. We expect that the general applicability and practicality of this CCS approach will increase the throughput of many chemical development programs by providing time-efficient and cost-effective screening tools that streamline current asymmetric reaction discovery and optimization protocols.

## MATERIALS AND METHODS

### General procedure

A solution of AD-mix- $\beta$  (179.0 mg), methanesulfonamide (13.2 mg, 0.14 mmol), and *trans*-stilbene (25 mg, 0.14 mmol) was vigorously stirred in 8 ml of a 1:1 water/*t*-BuOH mixture overnight. Excess Na<sub>2</sub>SO<sub>3</sub> was added, and stirring was continued for an additional hour. The reaction mixture was quenched with CH<sub>2</sub>Cl<sub>2</sub>, washed with 2 M NaOH, and dried over MgSO<sub>4</sub>. The reaction was also carried out as described above with stilbene (25 mg, 0.14 mmol), K<sub>3</sub>Fe(CN)<sub>6</sub> (137.0 mg, 0.42 mmol), K<sub>2</sub>CO<sub>3</sub> (57.6 mg, 0.42 mmol), OsO<sub>4</sub> (14.1  $\mu$ l, 0.0013 mmol), cinchonine (1.0 mg, 0.0031 mmol), and methanesulfonamide (13.2 mg, 0.14 mmol) at room temperature. We used the crude product of these reactions to determine the yield, ee, and absolute configuration of hydrobenzoin with **1** as described above and in the Supplementary Materials. For comparison, the reaction mixtures were purified by flash chromatography on silica gel (3:1 CH<sub>2</sub>Cl<sub>2</sub>/EtOAc) to isolate pure hydrobenzoin as colorless crystals and to determine the yield and ee. The ee was determined by HPLC on a Chiralcel OJ column using hexanes/*i*-PrOH (92:8, v/v) as mobile phase at 1 ml/min,  $t_1$  (S,S) = 19.4 min, and  $t_2$  (R,R) = 23.4 min.

## SUPPLEMENTARY MATERIALS

Supplementary material for this article is available at <http://advances.sciencemag.org/cgi/content/full/2/2/e1501162/DC1>

General information  
 Synthetic procedures  
 Enantioselective sensing experiments  
 Quantitative ee and concentration analysis  
 Ee and concentration analysis of hydrobenzoin **25** obtained by asymmetric Sharpless dihydroxylation  
 MS analysis of the in situ complex formation  
 Analysis of the sensing mechanism with the stereodynamic Ti complex  
 Crystallography  
 Scheme S1. General synthesis of **1**.  
 Fig. S1. <sup>1</sup>H and <sup>13</sup>C NMR spectra of **2** in CDCl<sub>3</sub>.  
 Fig. S2. <sup>1</sup>H and <sup>13</sup>C NMR spectra of **3** in CDCl<sub>3</sub>.  
 Fig. S3. <sup>1</sup>H and <sup>13</sup>C NMR spectra of **1** in CDCl<sub>3</sub>.  
 Fig. S4. Structures of substrates **4** to **29**.  
 Fig. S5. CD response of the zinc complex of **1** to chiral diamines, amines, and amino alcohols.  
 Fig. S6. CD response of the zinc complex of **1** to chiral amino acids.  
 Fig. S7. CD response of the aluminum complex of **1** to carboxylic acids.  
 Fig. S8. CD response of the titanium complex of **1** to chiral diols.  
 Fig. S9. CD spectra obtained from **1**, (S)-**19**, and Me<sub>3</sub>Al (solid red) and from **1**, (S)-**19**, and B(OMe)<sub>3</sub> (dashed red).  
 Fig. S10. CD spectra of the Zn complex obtained with **1** and scalemic samples of **14**.  
 Fig. S11. Exponential relationship between the CD amplitudes at 338 nm (blue), 385 nm (red), and 445 nm (green) and the ee of **14**.  
 Fig. S12. Fluorescence spectra of the complexes formed from **1**, Et<sub>2</sub>Zn, and varying concentrations of **14** from 0 to 100 mol% (blue) and 120 to 200 mol% (red).  
 Fig. S13. Fluorescence intensity (I) measured at 600 nm plotted against the ratio of [**14**]/[**1**].  
 Fig. S14. Curve fitting of the fluorescence emission at 600 nm.  
 Fig. S15. CD spectra of the Ti complex obtained with **1** and scalemic samples of **25**.  
 Fig. S16. Linear relationship between the CD amplitudes at 375 nm (red) and 470 nm (blue) and the ee of **25**.  
 Fig. S17. Fluorescence spectra of the complexes formed from **1**, Ti(O*i*-Pr)<sub>4</sub>, and varying concentrations of **25** from 0 to 100 mol% (blue) and 120 to 160 mol% (red).  
 Fig. S18. Fluorescence intensity (I) measured at 585 nm plotted against the ratio of [**25**]/[**1**].  
 Fig. S19. Curve fitting of the fluorescence emission at 585 nm.  
 Fig. S20. Asymmetric Sharpless dihydroxylation of *trans*-stilbene.  
 Fig. S21. HPLC separation of the product obtained with AD-mix- $\beta$  at 0°C on a Chiralcel OJ column using hexanes/*i*-PrOH (92:8, v/v) as mobile phase.  
 Fig. S22. HPLC separation of the product obtained with AD-mix- $\beta$  at 25°C on a Chiralcel OJ column using hexanes/*i*-PrOH (92:8, v/v) as mobile phase.  
 Fig. S23. HPLC separation of the product obtained with AD-mix- $\beta$  at 50°C on a Chiralcel OJ column using hexanes/*i*-PrOH (92:8, v/v) as mobile phase.  
 Fig. S24. HPLC separation of the product obtained with cinchonine at 25°C on a Chiralcel OJ column using hexanes/*i*-PrOH (92:8, v/v) as mobile phase.  
 Fig. S25. MS spectrum of the complex obtained from **1**, Et<sub>2</sub>Zn, and (1*R*,2*R*)-**4**.  
 Fig. S26. MS spectrum of the complex obtained from **1**, Et<sub>2</sub>Zn, and (1*R*,2*S*)-**10**.  
 Fig. S27. MS spectrum of the complex obtained from **1**, Et<sub>2</sub>Zn, and (1*R*,2*S*)-**14**.  
 Fig. S28. MS spectrum of the complex obtained from **1**, Me<sub>3</sub>Al, and (R)-**23**.  
 Fig. S29. MS spectrum of the complex obtained from **1**, Ti(O*i*-Pr)<sub>4</sub>, and (1*R*,2*R*)-**25**.  
 Fig. S30. MS spectrum of the complexes obtained from **1**, Ti(O*i*-Pr)<sub>4</sub>, and a mixture of (1*S*,2*S*)-**25** and (2*R*,3*R*)-**26**.  
 Fig. S31. MS spectrum of the complexes obtained from **1**, Ti(O*i*-Pr)<sub>4</sub>, (1*S*,2*S*)-**25**, and (2*S*,3*S*)-**26**.  
 Fig. S32. Excerpt of the NMR spectrum showing the methine proton septet in [Ti(O*i*-Pr)<sub>4</sub>] (red) after addition of one equivalent of **1** (green) and upon addition of one equivalent of **25** (blue).  
 Fig. S33. Excerpt of the NMR spectrum showing the methyl doublet of [Ti(O*i*-Pr)<sub>4</sub>] (red) after addition of one equivalent of **1** (green) and upon addition of one equivalent of **25** (blue).  
 Fig. S34. CD intensity at 375 nm (triangle) and 470 nm (diamond) for the complex obtained from Ti(O*i*-Pr)<sub>4</sub>, **1**, and (1*R*,2*R*)-**25** (blue) and for (1*S*,2*S*)-**25** (red).  
 Fig. S35. X-ray structure of bis(2-methoxy-1-naphthyl)ketone, **3**.  
 Fig. S36. X-ray structure of bis(2-hydroxy-1-naphthyl)ketone, **1**.  
 Table S1. Ee determination of *N*-methylephedrine.  
 Table S2. Experimentally determined concentrations of five samples of varying concentrations.  
 Table S3. Ee determination of hydrobenzoin.  
 Table S4. Experimentally determined concentrations of five samples of varying concentrations of **25** using the fluorescence response at 600 nm.  
 Table S5. Comparison of calculated and actual ee and concentration values of hydrobenzoin obtained by asymmetric Sharpless dihydroxylation.

## REFERENCES AND NOTES

1. A. McNally, C. K. Prier, D. W. C. MacMillan, Discovery of an  $\alpha$ -amino C–H arylation reaction using the strategy of accelerated serendipity. *Science* **334**, 1114–1117 (2011).
2. A. B. Santanilla, E. L. Regalado, T. Pereira, M. Shevlin, K. Bateman, L.-C. Campeau, J. Schneeweis, S. Berritt, Z.-C. Shi, P. Nantermet, Y. Liu, R. Helmy, C. J. Welch, P. Vachal, I. W. Davies, T. Cernak, S. D. Dreher, Nanomole-scale high-throughput chemistry for the synthesis of complex molecules. *Science* **347**, 49–53 (2015).
3. M. R. Friedfeld, M. Shevlin, J. M. Hoyt, S. W. Krska, M. T. Tudge, P. J. Chirik, Cobalt precursors for high-throughput discovery of base metal asymmetric alkene hydrogenation catalysts. *Science* **342**, 1076–1080 (2013).
4. K. D. Collins, T. Gensch, F. Glorius, Contemporary screening approaches to reaction discovery and development. *Nat. Chem.* **6**, 859–871 (2014).
5. X. Gao, H. B. Kagan, One-pot multi-substrate screening in asymmetric catalysis. *Chirality* **10**, 120–124 (1998).
6. C. Wolf, P. A. Hawes, A high-throughput screening protocol for fast evaluation of enantioselective catalysts. *J. Org. Chem.* **67**, 2727–2729 (2002).
7. A. Duursma, A. J. Minnaard, B. L. Feringa, One-pot multi-substrate enantioselective conjugate addition of diethylzinc to nitroalkenes. *Tetrahedron* **58**, 5773–5778 (2002).
8. M. T. Reetz, M. H. Becker, K. M. Kühling, A. Holzwarth, Time-resolved IR-thermographic detection and screening of enantioselectivity in catalytic reactions. *Angew. Chem. Int. Ed.* **37**, 2647–2650 (1998).
9. M. T. Reetz, A. Eipper, P. Tielmann, R. Mynott, A practical NMR-based high-throughput assay for screening enantioselective catalysts and biocatalysts. *Adv. Synth. Catal.* **344**, 1008–1016 (2002).
10. M. A. Evans, J. P. Morken, Isotopically chiral probes for in situ high-throughput asymmetric reaction analysis. *J. Am. Chem. Soc.* **124**, 9020–9021 (2002).
11. J. Guo, J. Wu, G. Siuzdak, M. G. Finn, Measurement of enantiomeric excess by kinetic resolution and mass spectrometry. *Angew. Chem. Int. Ed.* **38**, 1755–1758 (1999).
12. M. T. Reetz, M. H. Becker, H.-W. Klein, D. Stöckigt, A method for high-throughput screening of enantioselective catalysts. *Angew. Chem. Int. Ed.* **38**, 1758–1761 (1999).
13. C. Ebner, C. A. Müller, C. Markert, A. Pfaltz, Determining the enantioselectivity of chiral catalysts by mass spectrometric screening of their racemic forms. *J. Am. Chem. Soc.* **133**, 4710–4713 (2011).
14. F. Taran, C. Gauchet, B. Mohar, S. Meunier, A. Valleix, P. Y. Renard, C. Créminon, J. Grassi, A. Wagner, C. Mioskowski, High-throughput screening of enantioselective catalysts by immunoassay. *Angew. Chem. Int. Ed.* **41**, 124–127 (2002).
15. J. A. Friest, S. Broussy, W. J. Chung, D. B. Berkowitz, Combinatorial catalysis employing a visible enzymatic beacon in real time: Synthetically versatile (pseudo)halometalation/carbocyclizations. *Angew. Chem. Int. Ed.* **50**, 8895–8899 (2011).
16. T. A. Feagin, D. P. V. Olsen, Z. C. Headman, J. M. Heemstra, High-throughput enantiopurity analysis using enantiomeric DNA-based sensors. *J. Am. Chem. Soc.* **137**, 4198–4206 (2015).
17. D. Leung, S. O. Kang, E. V. Anslyn, Rapid determination of enantiomeric excess: A focus on optical approaches. *Chem. Soc. Rev.* **41**, 448–479 (2012).
18. C. Wolf, K. W. Bentley, Chirality sensing using stereodynamic probes with distinct electronic circular dichroism output. *Chem. Soc. Rev.* **42**, 5408–5424 (2013).
19. T. Kurtán, N. Nesnas, F. E. Koehn, Y.-Q. Li, K. Nakanishi, N. Berova, Chiral recognition by CD-sensitive dimeric zinc porphyrin host. 2. Structural studies of host–guest complexes with chiral alcohol and monoamine conjugates. *J. Am. Chem. Soc.* **123**, 5974–5982 (2001).
20. S. Nieto, V. M. Lynch, E. V. Anslyn, H. Kim, J. Chin, High-throughput screening of identity, enantiomeric excess, and concentration using MLCT transitions in CD spectroscopy. *J. Am. Chem. Soc.* **130**, 9232–9233 (2008).
21. L. You, J. S. Berman, E. V. Anslyn, Dynamic multi-component covalent assembly for the reversible binding of secondary alcohols and chirality sensing. *Nat. Chem.* **3**, 943–948 (2011).
22. M. Anyika, H. Gholami, K. D. Ashtekar, R. Acho, B. Borhan, Point-to-axial chirality transfer—A new probe for “sensing” the absolute configurations of monoamines. *J. Am. Chem. Soc.* **136**, 550–553 (2014).
23. L. A. Joyce, M. S. Maynor, J. M. Dagna, G. M. da Cruz, V. M. Lynch, J. W. Canary, E. V. Anslyn, A simple method for the determination of enantiomeric excess and identity of chiral carboxylic acids. *J. Am. Chem. Soc.* **133**, 13746–13752 (2011).
24. D. P. Iwaniuk, C. Wolf, A stereodynamic probe providing a chiroptical response to substrate controlled induction of an axially chiral arylacetylene framework. *J. Am. Chem. Soc.* **133**, 2414–2417 (2011).
25. K. W. Bentley, C. Wolf, Stereodynamic chemosensor with selective circular dichroism and fluorescence readout for in situ determination of absolute configuration, enantiomeric excess and concentration of chiral compounds. *J. Am. Chem. Soc.* **135**, 12200–12203 (2013).
26. J. Ściebura, P. Skowronek, J. Gawronski, Trityl ethers: Molecular bevel gears reporting chirality through circular dichroism spectra. *Angew. Chem. Int. Ed.* **48**, 7069–7072 (2009).
27. S. J. Wezenberg, G. Salassa, E. C. Escudero-Adán, J. Benet-Buchholz, A. W. Kleij, Effective chirogenesis in a bis(metallosalphen) complex through host–guest binding with carboxylic acids. *Angew. Chem. Int. Ed.* **50**, 713–716 (2011).
28. Z.-B. Li, J. Lin, Y.-C. Qin, L. Pu, Enantioselective fluorescent recognition of a soluble “supported” chiral acid: Toward a new method for chiral catalyst screening. *Org. Lett.* **7**, 3441–3444 (2005).
29. T. Matsumoto, Y. Urano, Y. Takahashi, Y. Mori, T. Terai, T. Nagano, In situ evaluation of kinetic resolution catalysts for nitroaldol by rationally designed fluorescence probe. *J. Org. Chem.* **76**, 3616–3625 (2011).
30. G. E. Tumambac, C. Wolf, Enantioselective analysis of an asymmetric reaction using a chiral fluorosensor. *Org. Lett.* **7**, 4045–4048 (2005).
31. D. Leung, E. V. Anslyn, Transitioning enantioselective indicator displacement assays for  $\alpha$ -amino acids to protocols amenable to high-throughput screening. *J. Am. Chem. Soc.* **130**, 12328–12333 (2008).
32. S. H. Shabbir, C. J. Regan, E. V. Anslyn, A general protocol for creating high-throughput screening assays for reaction yield and enantiomeric excess applied to hydrobenzoin. *Proc. Natl. Acad. Sci. U.S.A.* **106**, 10487–10492 (2009).
33. S. Nieto, J. M. Dagna, E. V. Anslyn, A facile circular dichroism protocol for rapid determination of enantiomeric excess and concentration of chiral primary amines. *Chemistry* **16**, 227–232 (2010).
34. L. A. Joyce, E. C. Sherer, C. J. Welch, Imine-based chiroptical sensing for analysis of chiral amines: From method design to synthetic application. *Chem. Sci.* **5**, 2855–2861 (2014).
35. P. Zhang, C. Wolf, Sensing of the concentration and enantiomeric excess of chiral compounds with tropos ligand derived metal complexes. *Chem. Commun.* **49**, 7010–7012 (2013).
36. K. W. Bentley, Y. G. Nam, J. M. Murphy, C. Wolf, Chirality sensing of amines, diamines, amino acids, amino alcohols, and  $\alpha$ -hydroxy acids with a single probe. *J. Am. Chem. Soc.* **135**, 18052–18055 (2013).
37. M. Kitamura, S. Okada, S. Suga, R. Noyori, Enantioselective addition of dialkylzincs to aldehydes promoted by chiral amino alcohols. Mechanism and nonlinear effect. *J. Am. Chem. Soc.* **111**, 4028–4036 (1989).
38. C. Girard, H. B. Kagan, Nonlinear effects in asymmetric synthesis and stereoselective reactions: Ten years of investigation. *Angew. Chem. Int. Ed.* **37**, 2922–2959 (1998).
39. C. Diebold, P. Mobian, C. Huguenard, L. Allouche, M. Henry, Synthesis and characterization of a monomeric octahedral  $C_2$ -symmetric titanium complex bearing two 3,3'-diphenyl-2,2'-biphenol ligands. *Dalton Trans.* 10178–10180 (2009).
40. J. P. Corden, W. Errington, P. Moore, M. G. H. Partridge, M. G. H. Wallbridge, Synthesis of di-, tri- and penta-nuclear titanium(IV) species from reactions of titanium(IV) alkoxides with 2,2'-biphenol ( $H_2L^1$ ) and 1,1'-binaphthol ( $H_2L^2$ ); crystal structures of  $[Ti_3(\mu_2-OPr^i)_2(OPr^i)_8L^1]$ ,  $[Ti_3(OPr^i)_6L^1_3]$ ,  $[Ti_5(\mu_3-O)_2(\mu_2-OR)_2(OR)_6L^1_4]$  ( $R = OPr^i, OBU^i$ ) and  $[Ti_2(OPr^i)_4L^2_2]$ . *Dalton Trans.* 1846–1851 (2004).
41. K. B. Sharpless, W. Amberg, Y. L. Bennani, G. A. Crispino, J. Hartung, K. S. Jeong, H. L. Kwong, K. Morikawa, Z. M. Wang, The osmium-catalyzed asymmetric dihydroxylation: A new ligand class and a process improvement. *J. Org. Chem.* **57**, 2768–2771 (1992).

**Acknowledgments:** We thank the U.S. National Science Foundation (grant CHE 1464547) for financial support. **Funding:** This work was supported by the U.S. National Science Foundation (CHE 1464547). **Author contributions:** C.W. planned the project. P.Z. designed and synthesized compound **1**. K.W.B. performed all CD and fluorescence experiments, MS, NMR, x-ray analysis, and the CCS assays. C.W. and K.W.B. discussed the results and designed the experiments. C.W. and K.W.B. wrote the manuscript. C.W., P.Z., and K.W.B. wrote the Supplementary Materials. **Competing interests:** The authors declare that they have no competing interests. **Data and materials availability:** All data needed to evaluate the conclusions in this article are present in the paper and/or the Supplementary Materials. Additional data related to this paper may be requested from the authors.

Submitted 25 August 2015  
Accepted 2 December 2015  
Published 12 February 2016  
10.1126/sciadv.1501162

**Citation:** K. W. Bentley, P. Zhang, C. Wolf, Miniature high-throughput chemosensing of yield, ee, and absolute configuration from crude reaction mixtures. *Sci. Adv.* **2**, e1501162 (2016).